

A REVISED MASS MODEL FOR THE ANDROMEDA GALAXY

MARC S. SEIGAR, AARON J. BARTH AND JAMES S. BULLOCK

Center for Cosmology, Department of Physics & Astronomy, University of California, Irvine, 4129 Frederick Reines Hall, Irvine, CA 92697-4575

Draft version February 7, 2020

ABSTRACT

We present an updated mass model for M31 that utilizes the 2MASS K-band image of the Andromeda galaxy, a revised estimate of the stellar mass-to-light ratio (M/L), and observed rotation curve data from a variety of sources. We examine cases where the dark matter follows a pure NFW profile and where an initial NFW halo contracts adiabatically in response to the formation of the galaxy. We find that the rotation curve data are most consistent with an adiabatically contracted NFW halo with an initial concentration $c_{\text{vir}} = 12.0$ and virial mass $8.7 \times 10^{11} M_{\odot}$. Models without adiabatic contraction are disfavored at high significance and specifically have difficulty reproducing the decline in rotation velocity at $r > 15$ kpc. Our best-fit M31 virial mass is a factor of ~ 2 smaller than the most recent estimate from rotation curve fitting by Klypin et al. (2002). The difference is driven by our updated baryonic mass model. The best-fit mass is consistent with published estimates from Andromeda Stream kinematics, satellite galaxy radial velocities, and planetary nebulae studies. Finally, using the known linear correlation between rotation curve shear and spiral arm pitch angle, we show that the stellar spiral arm pitch angle of M31 (which cannot be deduced from imaging data due to the galaxy's inclination) is $P = 24^{\circ}7 \pm 4^{\circ}4$.

Subject headings: dark matter — galaxies: fundamental parameters — galaxies: halos — galaxies: individual (M31) — galaxies: spiral — galaxies: structure

1. INTRODUCTION

Modeling the mass distribution of M31 is a classical problem that has seen many past iterations (e.g., Einasto 1972; Kent et al. 1989; Klypin et al. 2002). Recently, a deep near-infrared K_s -band image of M31 has become available through the 2MASS survey (Jarrett et al. 2003). With updated mass-to-light (M/L) ratios from Bell et al. (2003), this allows for a more accurate determination of the baryonic mass distribution in M31 than has ever been determined previously.

Because M31 can be studied in exquisite detail, it provides a crucial testing ground for ideas in galaxy formation (Kent 1989; Evans & Wilkinson 2000). A problem of particular relevance for Λ CDM is the Tully-Fisher zero-point problem, which refers to the fact that standard models cannot reproduce the relation between galaxy luminosity and circular velocity (Tully & Fisher 1977) without over-producing the number density of galaxies at fixed luminosity (e.g. Gonzalez et al. 2000; Cole et al. 2000; Benson et al. 2003; Yang et al. 2003). Another problem of related concern is the cusp/concentration problem — namely that dark-matter dominated galaxy rotation curves seem to rise more slowly than predicted in Λ CDM (Moore 1994; Flores & Primack 1994; Moore et al. 1999; van den Bosch & Swaters 2001; Blais-Ouellette et al. 2001; Alam et al. 2002; Swaters et al. 2003; Simon et al. 2005; Dutton et al. 2005; Kuzio de Naray et al. 2006). It remains to be seen whether these problems point to some unaccounted for process in galaxy formation (e.g. Dutton et al. 2006) or to some new physics of cosmological relevance (Kaplinghat et al. 2000; Zentner & Bullock 2002; Kaplinghat 2005; Cembranos et al. 2005; Strigari, Kaplinghat & Bullock 2006; Gnedin et al. 2006).

Recently, Dutton et al. (2006) and Gnedin et al. (2006) revisited the Tully-Fisher problem using two large well-defined samples of disk-dominated (late-type) galaxies. They both took as a starting point the “standard” model of disk formation, which assumes that initial Navarro, Frenk & White (1997; hereafter NFW) dark halos respond to disk formation via adiabatic contraction (AC) (Blumenthal et al. 1986; Gnedin et al. 2004; Sellwood & McGaugh 2005; Choi et al. 2006). Both groups conclude that the Tully-Fisher zero point cannot be explained if initial NFW halos have concentrations as high as those expected for Λ CDM with $\sigma_8 \simeq 0.9$ (with $c \sim 12$ for M31-size halos, e.g. Bullock et al. 2001a, Macciò et al. 2006). Both sets of authors agree that the problem could be alleviated if AC did not operate (e.g. Somerville & Primack 1999) and Dutton et al. (2006) go on to advocate a model where disk formation induces an *expansion* in the underlying halo density structure. In contrast, Gnedin et al. (2006) argue that AC is a fundamental prediction in galaxy formation and instead suggest that the cosmology be changed to favor lower halo concentrations (e.g., Zentner & Bullock 2002) or that the IMF is lighter than the standard Kroupa assumption.

Given the fundamental issues at hand, the question of whether AC occurs in nature is of significant interest. Theory certainly favors the idea that halos contract. Indeed, halo contraction must occur when the infall of baryons is smooth and adiabatic (e.g. Blumenthal et al. 1986; Ryden & Gunn 1987; Sellwood & McGaugh 2005) and simulations suggest that dark halos will contract even when galaxies or galaxy clusters form quickly from an irregular collapse (Barnes 1987; Flores et al. 1993; Jesseit et al. 2002; Gnedin et al. 2004; Sellwood & McGaugh 2005; Choi et al. 2006; Weinberg et al. 2006). On the other hand, there is very little observa-

tional evidence that halo contraction actually occurs in nature. For example, Zappacosta et al. (2006) performed a detailed XMM study of the radio-quiet galaxy cluster A2589 and conclude that an NFW halo + AC model cannot explain the data but that a pure NFW halo provides a remarkable fit down to $\sim 1\%$ of the halo's virial radius. Similarly, an investigation of seven elliptical galaxies with *Chandra* by the same group (Humphrey et al. 2006) finds that AC degrades the mass profile fits significantly unless strong deviations from a Kroupa IMF are allowed. Also, Kassin et al. (2006a, b) find that the rotation curves of 32 out of 34 of the bright spiral galaxies they study are better fit without adiabatic contraction.

Klypin et al. (2002) have shown that the observed rotation curve of M31 is best explained with a halo model that includes AC. Given the updated M/L ratios and the availability of a 2MASS K_s -band image, it is now appropriate to revisit this question. In what follows we also show that the rotation curve of M31 strongly favors AC. We show that the fall-off in rotation velocity beyond ~ 15 kpc cannot be explained without AC for any reasonable NFW concentration ($c \lesssim 40$). Moreover, the best-fit AC model has a fairly average NFW concentration, $c_{\text{vir}} = 12$, for typical, $\sigma_8 = 0.9$, Λ CDM halos (Bullock et al. 2001a, Macciò et al. 2006). When viewed in the context of Λ CDM, M31 provides perhaps the strongest evidence that AC does occur in some cases. We speculate on the implications of this result in the conclusion section.

Throughout this paper we assume a flat Λ CDM cosmology with $\Omega_m = 0.27$ and a Hubble constant of $H_0 = 75 \text{ km s}^{-1} \text{ Mpc}^{-1}$. We relate virial masses (M_{vir}) and radii (R_{vir}) assuming a virial over-density relative to *average* of $\Delta_{\text{vir}} = 347$. ¹ At times we quote baryon fractions relative to the universal value with $f_b = \Omega_b/\Omega_m = 0.16$.

We adopt a distance of 784 kpc to M31 (Holland 1998). As a result, an angular distance of $1'$ is equivalent to a distance of 228 pc.

2. DATA

We make use of the 2MASS K_s -band image of M31 (Jarrett et al. 2003), with a total integration time of 7.8 seconds per position for the K_s -band image. ² The image is 2.8 deg^2 on the sky, with a pixel scale of $1''$. We also use the $B - R$ color profile of Walterbos & Kennicutt (1989).

We adopt the rotation curve data from several sources. In one case (M1) we adopt the H α rotation data out to 25 kpc from Rubin & Ford (1970) and extend the rotation curve to 35 kpc using H I data from Carignan et al. (2006). In another case (M2) we use the CO rotational velocities from Loinard et al. (1995) and the H I from Brinks & Burton (1984) to construct an observed rotation curve out to a 30 kpc radius. This was the rotation curve adopted by Klypin et al. (2002) in their M31 model. We adopt M1 as our fiducial case here because Rubin & Ford published errors on their observed velocities. However, as we show below, both cases yield consistent results. In both cases we take into account the

¹ Specifically we use $R_{\text{vir}} = 206h^{-1}(M_{\text{vir}}/10^{12}h^{-1}\text{M}_\odot)^{1/3}$ kpc.

² See <http://www.ipac.caltech.edu/2mass/releases/allsky/doc/> for a description of the 2MASS survey and data access.

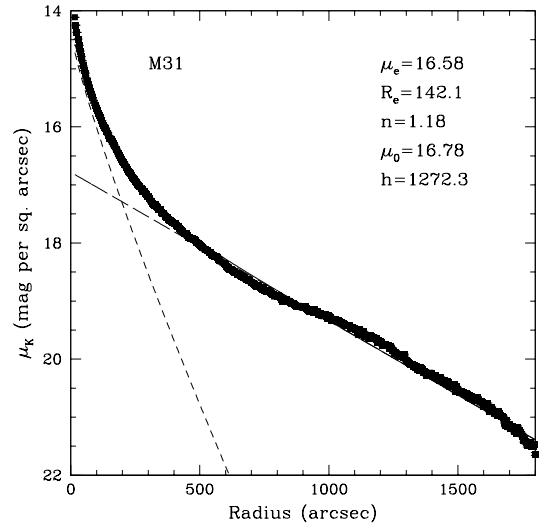


FIG. 1.— The 2MASS K_s -band surface brightness profile of M31 with decomposition into Bulge and Disk components. The Bulge has been fitted with a Sérsic model (short dashed line) and the Disk has been fitted with an exponential model (long dashed line). In this paper we adopt an M31 distance (781 kpc) such that $100''$ is equivalent to 380 pc.

presence of a $10^8 M_\odot$ supermassive black hole (Bender et al. 2005) and the H I gas distribution (Carignan et al. 2006).

3. MASS MODELING OF M31

3.1. The baryonic contribution

Our goal is to determine the best possible mass model for M31. We perform a bulge-disk decomposition in order to estimate the baryonic contribution to the rotation curve. We then determine several possible mass models. The best fit model is determined by minimizing the reduced- χ^2 , in a fit to the observed rotation curve.

We first extract the surface brightness profile of M31 using the 2MASS K_s -band image, and the IRAF `ellipse` routine, which fits ellipses to an image using an iterative method described by Jedrzejewski (1987). In order to mask out foreground stars and satellite galaxies, SExtractor (Bertin & Arnouts 1996) was used. An inclination correction was then applied to the surface brightness profile (see de Jong 1996; Seigar & James 1998a) as follows

$$\mu_i = \mu - 2.5C \log\left(\frac{a}{b}\right) \quad (1)$$

where μ_i is the surface brightness when viewed at some inclination, i , μ is the corrected surface brightness, a is the major axis, b is the minor axis and C is a factor dependent on whether the galaxy is optically thick or thin; if $C = 1$ then the galaxy is optically thin; if $C = 0$ then the galaxy is optically thick. Seigar & James (1998a) and de Jong (1996) both use the optically thin case and we adopt this approach here. The surface brightness profile is also then corrected for a ~ 0.5 magnitude error in the 2MASS calculated zeropoint, due to the fact that the sky level is incorrect. Without this correction the surface brightness profile would be 0.5 magnitudes too faint (T. Jarrett, 2006, private communication).

From the surface brightness profile, we perform a one-dimensional bulge-disk decomposition, which employs

TABLE 1
M31 OBSERVATIONAL DATA

Parameter	Measurement
Hubble type	SA(s)b
Distance (kpc)	784
Position Angle of major axis (degrees)	45
Bulge effective radius, R_e (arcsec)	142.1 ± 7.6
Bulge effective radius, R_e (kpc)	0.53 ± 0.03
Bulge surface brightness at the effective radius, μ_e (K-mag arcsec $^{-2}$)	16.58 ± 0.86
Bulge Sérsic index, n	1.18 ± 0.08
Disk central surface brightness, μ_0 (K-mag arcsec $^{-2}$)	16.78 ± 0.93
Disk scale length, h (arcsec)	1272.3 ± 63.5
Disk scale length, h (kpc)	4.76 ± 0.27
Disk luminosity, L_{disk} (L_\odot)	$(7.01 \pm 0.69) \times 10^{10}$
Bulge-to-disk ratio, B/D	0.19 ± 0.01

NOTE. — Hubble type taken from de Vaucouleurs et al. (1991). Distance in kpc taken from Holland et al. (1998)

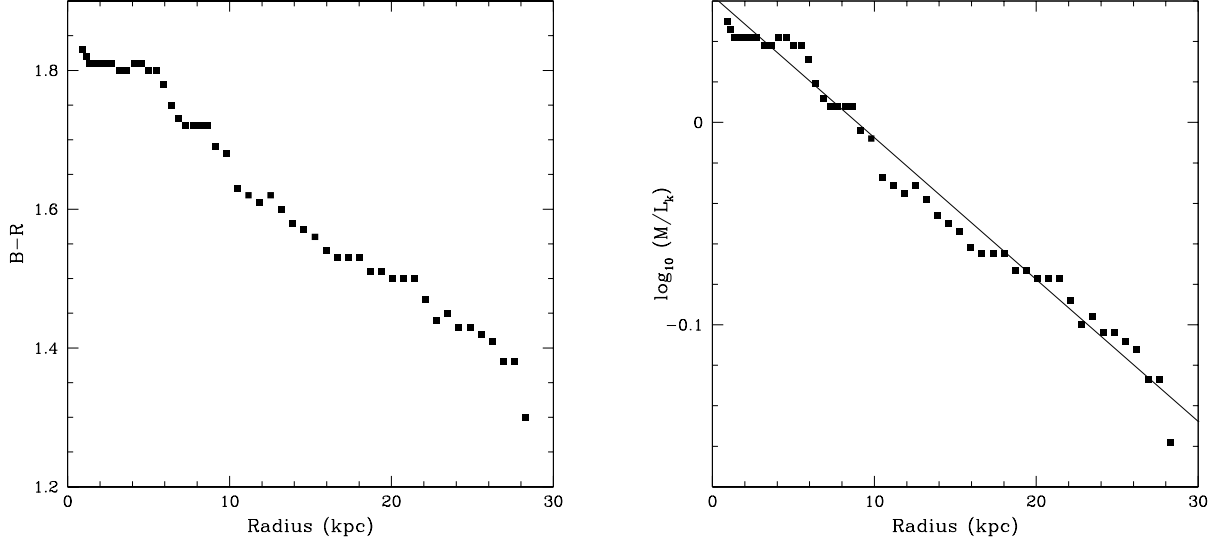


FIG. 2.— *Left:* $B - R$ color profile for M31 from Walterbos & Kennicutt (1987). *Right:* K_s -band M/L as a function of radius calculated using the $B - R$ color profile from Walterbos & Kennicutt (1987) and the M/L ratios of Bell et al. (2003).

the Sérsic model for the bulge component and an exponential law for the disk component (e.g. Andredakis et al. 1995; Seigar & James 1998a; Khosroshahi et al. 2000; D’Onofrio 2001; Graham 2001; Möllenhoff & Heidt 2001; see also Graham & Driver 2005 for a review). The Sérsic (1963, 1968) $R^{1/n}$ model is most commonly expressed as a surface brightness profile, such that

$$\mu(R) = \mu_e \exp \left\{ -b_n \left[\left(\frac{R}{R_e} \right)^{1/n} - 1 \right] \right\}, \quad (2)$$

where μ_e is the surface brightness at the effective radius R_e that encloses half of the total light from the model (Ciotti 1991; Caon et al. 1993). The constant b_n is defined in terms of the parameter n , which describes the overall shape of the light profile. When $n = 4$ the Sérsic model is equivalent to a de Vaucouleurs (1948, 1959) $R^{1/4}$ model and when $n = 1$ it is equivalent to an exponential model. The parameter b_n has been approximated by $b_n = 1.9992n - 0.3271$, for $0.5 < n < 10$ (Cappaccioli 1989; Prugniel & Simien 1997). The exponential model

for the disk surface brightness profile can be written as follows,

$$\mu(R) = \mu_0 \exp(-R/h), \quad (3)$$

where μ_0 is the disk central surface brightness and h is the disk scale length. Our bulge-disk decomposition ignores the inner 4'' of M31, which is dominated by an independent nuclear feature (Light et al. 1974). The results of the bulge-disk decomposition can be seen in Figure 1. Observational properties of M31 are derived from this bulge-disk decomposition and these are listed in Table 1.

Masses are assigned to the disk and bulge using a combination of stellar mass-to-light ratios from Bell et al. (2003) and $B - R$ colors from Walterbos & Kennicutt (1987). From the multicolor imaging data in Walterbos & Kennicutt (1987) we have fit a straight line to the $B - R$ color versus radius, which gives a slope of ~ 0.018 mag kpc $^{-1}$. The left panel of figure 2 shows the $B - R$ color profile of M31 from Walterbos & Kennicutt (1987). We then use the relation between $B - R$ color and K_s -band

M/L in Bell et al. (2003) to calculate a $\log(M/L)$ gradient of ~ 0.008 kpc $^{-1}$. The M/L as a function of radius is shown in the right panel of figure 2. The central color, $B - R \simeq 1.8$ is equivalent to a $(M/L) = 1.05 \pm 0.10$ in K_s -band solar units. We adopt this as our central value for the mass-to-light ratio in our rotation curve models and we allow it to vary by the 1σ error. We use the derived disk and bulge light profiles $L_K = L_{\text{disk}} + L_{\text{bulge}}$ to determine the stellar mass contribution to the rotation curve, $M_* = (M/L)L_K$.

3.2. Modeling the dark matter halo

A range of allowed dark matter halo masses and density profiles are now explored, using two extreme models for disk galaxy formation. In the first, we assume that the dark matter halo surrounding M31 has not responded significantly to the formation of the disk, i.e., adiabatic contraction does not occur (the “non-AC” model). In this case, the dark matter contribution to the rotation curve is described by a density profile similar to those found in dissipationless dark matter simulations (the NFW profile):

$$\rho(R) = \frac{\rho_s}{(R/R_s)(1 + R/R_s)^2} \quad (4)$$

where R_s is a characteristic “inner” radius, and ρ_s is a corresponding inner density. This is a two parameter function and is completely specified by choosing two independent parameters, e.g., the virial mass M_{vir} (or virial radius R_{vir}) and concentration $c_{\text{vir}} = R_{\text{vir}}/R_s$ (see Bullock et al. 2001a for a discussion). Similarly, given a virial mass M_{vir} and the dark matter circular velocity at any radius, the halo concentration c_{vir} is completely determined.

In the second class of models, we adopt the scenario of adiabatic contraction (AC) and specifically use the original scheme discussed by Blumenthal et al. (1986, hereafter B86; see also Bullock et al. 2001b and Pizagno et al. 2005). We also investigate the slightly revised scheme presented in Gnedin et al. (2004, hereafter G04). As we discuss below, the G04 scheme reproduces the outer slope of the observed rotation curve of M31, but needs a very high concentration to do so.

For each AC algorithm (B86 and G04) and for the non-AC model we generate a grid of final rotation curves. We vary the baryonic contribution to the rotation curve by allowing the bulge-disk decomposition parameters for h and L_{disk} and the central mass-to-light ratio of the galaxy (M/L) to range over their $\pm 1\sigma$ values (see Table 1 and the previous section). For each set of baryonic parameters we generate a range of dark halo models with total circular velocities at 2.2 disk scale length ($V_{2.2}$) that span the best-fit value for M31 ($V_{2.2} = 270$ km s $^{-1}$) quoted by Rubin & Ford (1970) by a wide margin: $200 < V_{2.2} < 340$ km s $^{-1}$. In practice, we achieve each $V_{2.2}$ value in our models by allowing the initial halo concentration to vary over $\sim 3.5\sigma$ of its expected range $c_{\text{vir}} = 3 - 40$ (Bullock et al. 2001a, Macciò et al. 2006) and then setting the halo virial mass M_{vir} necessary to reproduce the desired value of $V_{2.2}$. Finally, we determine the implied fraction of the mass in the system in the form of stars compared to that expected from the Universal baryon fraction, $f_* = M_*/(f_b M_{\text{vir}})$ and demand that f_* obeys

$0.01 f_b < f_* < f_b$. From this grid of choices, we derive best-fitting dark halo parameters by minimizing the reduced- χ^2 for our two choices of rotation curve data. These results are summarized in Table 2.

In the minimization of the reduced- χ^2 we assume that the errors on the observational data (i.e., the rotation velocities) are not correlated. Instead we assume that they are Gaussian in nature. This is an idealized simplification but allows a quantitative estimate of the relative goodness of fit between models. Furthermore, although error bars are not available for the “M2” curve, we assume 10% errors in the model fitting, as this is similar to the size of the errors quoted for the Rubin & Ford (1970) $\text{H}\alpha$ rotation curve. We therefore do not quote a reduced- χ^2 for the “M2” curve in Table 2. We then determine how consistent all the derived rotation curves are with each other, by adopting the formal best fitting rotation curve as our fiducial mass model. For our “M1” curve, the number of degrees of freedom in the fit is $\nu = 30$.

The M1 rotation curve from Rubin & Ford (1970) is shown by the solid squares with error bars in Figure 3 (*top left, top right, bottom right*) along with our best-fitting rotation curve models (solid lines). The data points are taken from the $\text{H}\alpha$ rotation velocities listed in Table 1 of Rubin & Ford (1970). ³ The contribution from stellar mass (short-dashed) and dark matter (long-dash) in each case is shown along with the rather minor contributions from neutral gas (dotted) and the central black hole (dot-dashed).

Overlaid in the *upper-left* panel of Figure 3 is our preferred model (overall reduced- $\chi^2 = 1.40$). The dark halo in this case *has undergone* adiabatic contraction according to the B86 prescription. Our best-fitting parameters are summarized in Table 2 under “M1 B86”. We determine the halo of M31 to have a total (dark+baryonic) virial mass of $M_{\text{vir}} = (8.7 \pm 0.7) \times 10^{11} M_{\odot}$ and an initial concentration $c_{\text{vir}} = 12.0 \pm 0.9$, i.e., the same as the initial concentration found by Klypin et al. (2002), but a virial mass almost a factor of 2 smaller. The quoted errors on the model parameters are found by finding the best-fit model to two extreme rotation curves, with the 1σ errors added to and subtracted from the observational data. We caution the reader that the the derived errors on the model parameters are a result of shifting the observed data systematically up and down by their 1σ error, i.e., the are not formal 1σ errors.

Clearly, the model rotation curve fits the data extremely well. The innermost data point from the observational rotation curve is significantly lower than the model. This can be explained by the recent strong evidence for a bar in M31 (Athanassoula & Beaton 2006; Beaton et al. 2006). This bar has been used to explain the minimum seen in the observed rotation curve at a radius of ~ 2.7 kpc (Athanassoula & Beaton 2006). It should also be noted that by a radius of $\sim 26 - 35$ kpc the rotational velocity has dropped to $\sim 225 - 230$ km s $^{-1}$, which is similar to the rotational velocities seen at radii of $25 - 35$ kpc in the H I rotation curve (Carignan et al. 2006; open triangles).

³ Figure 9 of Rubin & Ford (1970) also includes rotation velocities calculated from a narrow [N II] $\lambda 6583$ emission feature, for the region within 3 kpc. However, these velocities are not tabulated in their paper, and so we do not include them here.

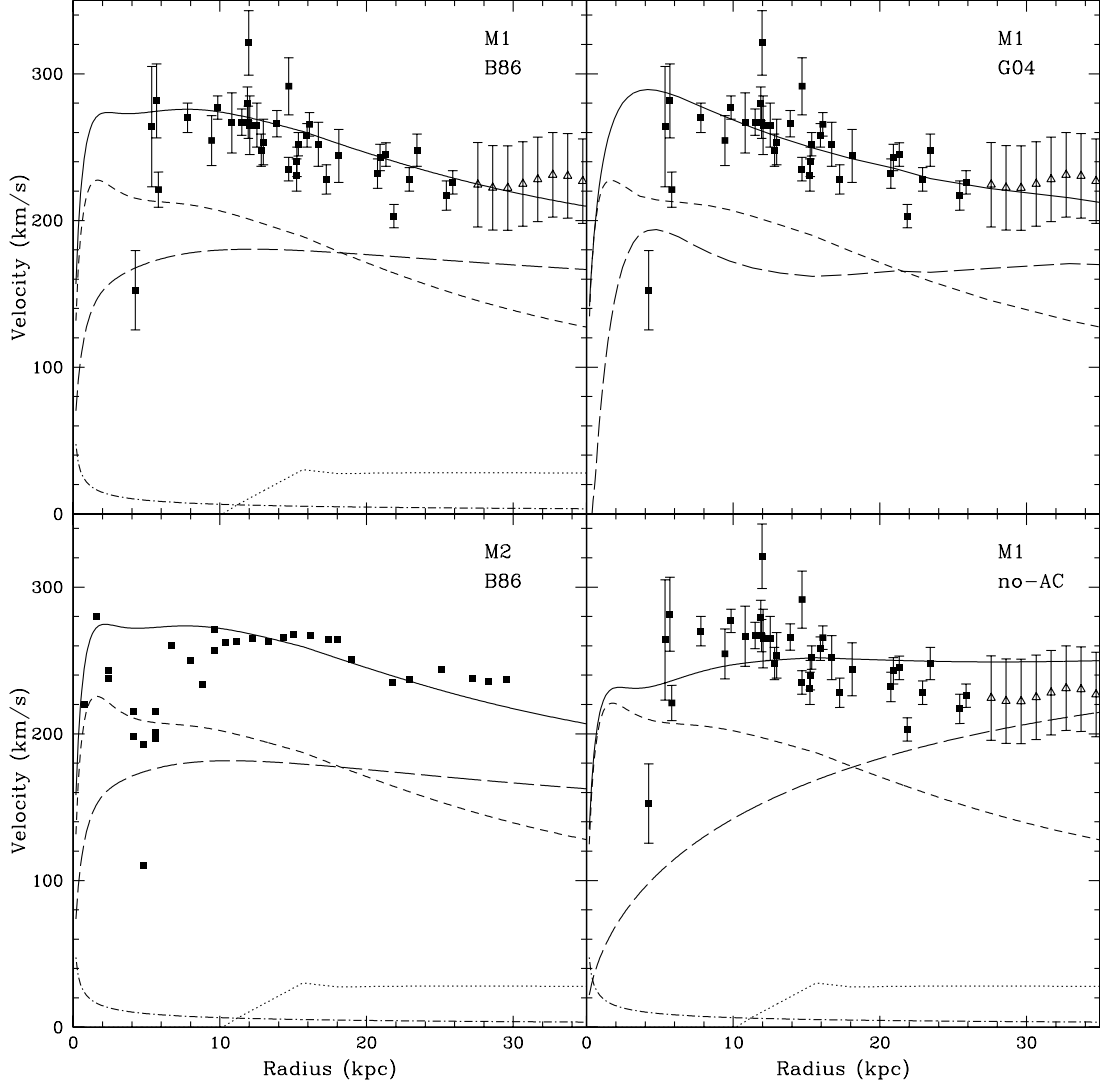


FIG. 3.— *Top left*: Rotation curve data (solid square points) from Rubin & Ford (1970) with the best fit model, with adiabatic contraction (M1 B86 model), overlaid (solid line). For comparison the H I rotation velocities (open triangles) from Carignan et al. (2006) are shown. The best fit rotation curve is decomposed into four components, the contribution from dark matter (long-dashed line), the contribution from baryonic matter (short-dashed line), the H I contribution (dotted line) from Carignan et al. (2006) and the contribution from the central $10^8 M_\odot$ black hole (dot-dashed line) from Bender et al. (2005). *Bottom left*: Rotation curve CO and H I data (solid square points) from Loillard et al. (1995) and Brinks & Burton (1984) respectively, as used by Klypin et al. (2002). The best fit model with adiabatic contraction (M2 B86 model) is overlaid (solid line). It is decomposed into four components as in the top left panel. *Top right*: The same as the top left panel, but with the best fitting model using a modified version of adiabatic contraction (M1 G04 model) as in Gnedin et al. (2004). *Bottom right*: The same as the top left panel, but with the best fitting model without an adiabatically contracted halo (M1 no-AC model).

The best-fitting model without adiabatic contraction is shown by the solid line in the *bottom right* panel of Figure 3. This, the non-AC model, was determined in exactly the same way as our best-fit B86 AC model. As listed in Table 2, the non-AC assumption requires a lower NFW concentration, $c = 7.0 \pm 0.6$ and a higher virial mass, $M_{\text{vir}} = (5.1 \pm 0.2) \times 10^{12} M_\odot$. Its best fitting rotation velocity at 2.2 disk scalelengths, $V_{2.2} = 250 \pm 5 \text{ km s}^{-1}$, clearly misses the actual rotation velocity of $\sim 270 \text{ km s}^{-1}$ at this radius ($\simeq 10 \text{ kpc}$). The difficulty arises from the fact that pure NFW dark halos produce extremely flat rotation curves. We were unable to find any set of halo parameters in the non-AC case that reproduced the peak in the observed H α rotation curve at $\sim 10 \text{ kpc}$, and the decline beyond this radius. The best-fitting pure

NFW halo is a worse fit with an overall reduced- $\chi^2 = 2.67$.

In Figure 4 we plot the reduced- χ^2 as a function of NFW concentration, c_{vir} , for both the “M1 B86” case (*left panel*) and the “M1 no-AC” case (*right panel*). In both of these cases we have fixed all other model parameters at their respective best-fit values. The difference in the reduced- χ^2 between these two models is $\Delta\chi^2/\nu=1.27$, where ν is the number of degrees of freedom in the fit, i.e. χ^2/ν is the definition of reduced- χ^2 . The standard deviation on the reduced- χ^2 is $\sim \sqrt{2/\nu} \simeq 0.25$. As a result the two models differ by about 5σ . The “M1-noAC” case can therefore be ruled out with 99.99% confidence. Also, the halo virial mass required for this model is $(5.1 \pm 0.2) \times 10^{12} M_\odot$. This is a very large halo

TABLE 2
M31 BEST FITTING MODELS

Parameter	M1 B86	M2 B86	M1 G04	M1 no-AC
Shear	0.52	0.52	0.56	0.44
$V_{2,2}$ (km s $^{-1}$)	275 \pm 5	275 \pm 5	275 \pm 5	250 \pm 5
Disk luminosity, L_{disk} (L_{\odot})	(7.0 \pm 0.7) \times 10 10			
Disk scale length, h (kpc)	4.70 \pm 0.05	4.70	4.93 \pm 0.05	4.93 \pm 0.05
Central disk mass-to-light ratio, M/L (K-band solar units)	0.95 \pm 0.02	0.95	0.95 \pm 0.02	0.95 \pm 0.02
Mass-to-light ratio gradient, $d(M/L)/dR$ (kpc $^{-1}$)	0.012	0.012	0.012	0.012
Initial NFW concentration, c_{vir}	12.0 \pm 0.9	14.0	40.0	7.0 \pm 0.6
Bulge-to-disk ratio, B/D	0.19 \pm 0.01	0.19	0.19 \pm 0.01	0.19 \pm 0.01
Virial mass, M_{vir} (M_{\odot})	(8.7 \pm 0.7) \times 10 11	7.4 \times 10 11	(8.0 \pm 0.7) \times 10 11	(5.1 \pm 0.2) \times 10 12
Dark matter concentration, c_{DM} , $R < 10$ kpc	9.1 \pm 1.3%	10.9%	8.6 \pm 1.1%	1.2 \pm 0.3%
Total mass concentration, c_{tot} , $R < 10$ kpc	20.5 \pm 2.4%	23.7%	16.0 \pm 2.3%	2.7 \pm 0.4%
Stellar baryon fraction, f_*	67.1 \pm 8.2%	80.5%	49.7 \pm 8.6%	11.5 \pm 1.7%
Reduced- χ^2	1.40	—	1.70	2.67

NOTE. — “M1 B86” is the best-fit model to the H α rotation curve from Rubin & Ford (1970) (M1) using the AC prescription of B86. “M2 B86” is the best-fit B86 model to a combination of the CO rotation velocities from Lionard et al. (1995) and the H I velocities from Brinks & Burton (1984). Although both models are consistent with each other, we favor “M1 B86”, because we know the observational errors associated with the Rubin & Ford (1970) rotation curve. “M1 G04” corresponds to the M1 data fit using the modified adiabatic contraction model of Gnedin et al. (2004) and “M1 no-AC”, uses the same data without adiabatic contraction. The “M1 no-AC” case is ruled out with $>99.99\%$ confidence, due to its higher reduced- χ^2 compared with the “M1 B86” case. The “M1 G04” case provides a good fit to the outer slope of the rotation curve (> 15 kpc), but it needs a very high concentration (as listed) to do so.

virial mass, and is several times larger than the typical virial mass derived for the Milky Way (e.g., Klypin et al. 2002; Dehnen et al. 2006). Given this, the low stellar baryon fraction of $f_* = 11.5 \pm 1.7\%$, and the high value of the reduced- χ^2 of the fit, it seems difficult to reconcile the halo of M31 with a pure NFW model.

An intermediate result is shown in the *upper right* panel of Figure 3. Here we use the AC model of G04, which produces less contraction than the B86 prescription. If the initial NFW concentration is held fixed at the same value as the best-fitting B86 case, i.e., $c_{vir} = 12$, then the G04 model overestimates the observed rotation curve at $r > 15$ kpc. The G04 model can only reproduce this outer slope with any degree of confidence when the initial halo has $c_{vir} = 40$ (i.e. the maximum allowed by our input prior). With this high concentration the reduced- χ^2 of the G04 model is 1.70. This model cannot be ruled out, but its halo concentration is higher than expected in Λ CDM (Bullock et al. 2001a, Macciò et al. 2006). We thus adopt the standard B86 AC prescription as our fiducial model.

For completeness, we also perform a fit to the same observed rotation curve that was used by Klypin et al. (2002) in their M31 mass decomposition. Our best fitting mass model is shown in the *bottom left* panel of Figure 3 (“M2 B86” in Table 2). Here we have adopted the B86 AC model. The initial NFW concentration in this case ($c_{vir} = 14$) is slightly higher than that favored by Klypin et al. (2002) and our “M1 B86” case. However, it is not a large difference, and at face value our “M1 B86” and “M2 B86” models are consistent with each other. As we discuss below, the difference between our result and that of Klypin et al. (2002) is driven mainly by our updated baryonic model.

Figure 5 shows the enclosed mass as a function of radius for our fiducial model (M1 B86). The fraction of mass contained within the central 10 kpc (the “central mass concentration” hereafter) is $c_{tot} = 20.5 \pm 2.4\%$. In absolute terms, the mass contained within 10 kpc is

$(17.8 \pm 2.3) \times 10^{10} M_{\odot}$. This is about 70% larger than that calculated by Rubin & Ford (1970), but it should be noted that they did not take into account non-circular orbits due to the presence of a bar, which we now know exists in M31. This would have the effect of increasing the mass contained within the bar region. The mass calculated within a 35 kpc radius from the H I rotation curve by Carignan et al. (2006) is $3.4 \times 10^{11} M_{\odot}$, similar to the mass derived from our best fit model within a 35 kpc of $(3.6 \pm 0.5) \times 10^{11} M_{\odot}$. Within a 31 kpc radius we find a mass of $(3.4 \pm 0.4) \times 10^{11} M_{\odot}$, which is similar to the mass of $2.8 \times 10^{11} M_{\odot}$ within the same radius found using kinematic data of planetary nebulae (Evans & Wilkinson 2000). The total implied stellar baryon fraction of this model is $f_* = 67.1 \pm 8.2\%$.

As mentioned above, the preferred total (dark+baryonic) virial mass for M31 is $(8.7 \pm 0.7) \times 10^{11} M_{\odot}$. This is consistent with the estimate of $\sim (7.9 \pm 0.5) \times 10^{11} M_{\odot}$ derived from satellite kinematics (Côté et al. 2000) and the total mass of $\sim 8 \times 10^{11} M_{\odot}$ from kinematics of the Andromeda Stream (Geehan et al. 2006). It is also close to, but lower than, the lower limit of $9 \times 10^{11} M_{\odot}$ derived from kinematics of halo stars (Chapman et al. 2006). Our favored virial mass is about half the value favored by the Klypin et al. (2002) analysis of the M31 rotation curve. This can be attributed to three differences in our analyses. First, Klypin et al. (2002) use the H I rotation curve of Brinks & Burton (1984) to find their best fitting model. In this study we use the H α rotation velocities of Rubin & Ford (1970). However, we find that this is not the major driver. We find that the model rotation velocities are consistent with those from the more recent H I study of Carignan et al. (2006), and when we fit to the same observed rotation curve as Klypin et al. (2002), we find that our best-fit model is consistent with our best-fit fit model to the Rubin & Ford (1970) curve. More importantly, Klypin et al. (2002) used the M/L ratios of Bell & de Jong (2002) to determine

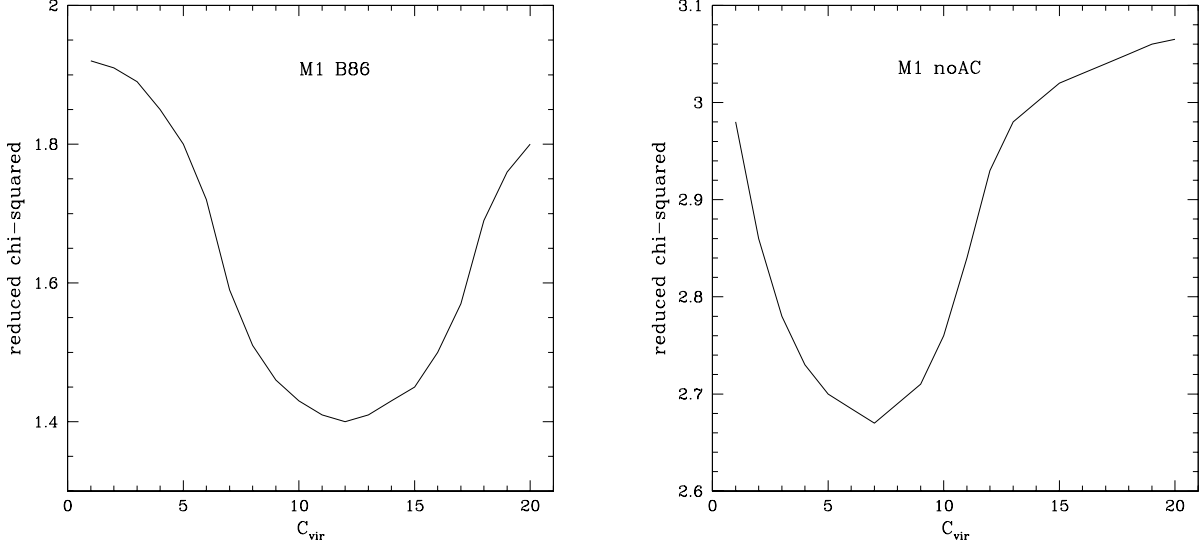


FIG. 4.— Reduced- χ^2 as a function of NFW concentration parameter, C_{vir} , for our fiducial “M1 B86” model (left panel) and our “M1 noAC” model (right panel). The best fitting values for concentration differ by more than 5σ between the two models.

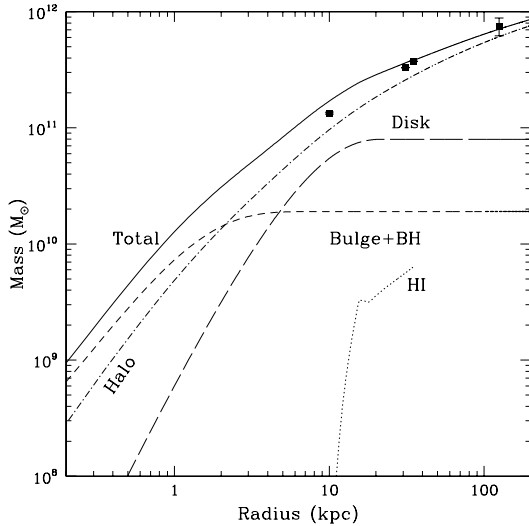


FIG. 5.— Enclosed mass as a function of radius for model M1 B86. The solid line indicates the total mass. Also indicated are the HI mass out to a 35 kpc radius (dotted line), the bulge+BH mass (short-dashed line), the disk mass (long-dashed line) and the halo mass (dot-dashed line). The data points indicate masses derived using other observational methods at fixed radii of 10 kpc, 31 kpc, 35 kpc and 125 kpc from Rubin & Ford (1970), Evans & Wilkinson (2000), Carignan et al. (2006) and Fardal et al. (2006) respectively.

the stellar mass from their bulge-disk decomposition. In this study we use the updated and more accurate M/L ratios of Bell et al. (2003), and this makes a large difference. For instance for $B - R \sim 1.4$ Bell & de Jong (2001) suggest a K_s -band $M/L \simeq 0.6$, whereas Bell et al. (2003) suggest a K_s -band $M/L \simeq 0.9$. This therefore makes a $\sim 50\%$ difference in the stellar mass of M31. This has a significant effect on the rotation curve. One other difference is that Klypin et al. (2002) perform a bulge-disk decomposition using an R band image, whereas we use a K_s -band image. Using a K_s -band image reduces the scatter in the allowed M/L ratios for any given color. Overall, we should therefore have a

more accurate estimate of the baryonic mass profile in M31. Indeed, if we adopt the baryonic mass profile of Klypin et al. (2002) and try to fit either to the H I or to the $H\alpha$ rotation curve, we find a best fitting model that is consistent with their result.

3.3. The spiral arm pattern of M31

Because M31 is a highly inclined galaxy, it is difficult to learn how tightly wound its spiral arm pattern is from imaging data. However, the spiral arm pitch angle can be estimated from the shear rate measured for the M31 rotation curve at 10 kpc using equation 4 from Seigar et al. (2006). This equation gives the line of best fit to the spiral arm pitch angle versus rotation curve shear correlation. The shear rate is defined as

$$S = \frac{A}{\omega} = \frac{1}{2} \left(1 - \frac{R}{V} \frac{dV}{dR} \right), \quad (5)$$

where A is the first Oort constant, ω is the angular velocity and V is the rotational velocity at radius R . The shear rate depends upon the shape of the rotation curve. For a rotation curve that remains flat the shear rate, $S = 0.5$, for a falling rotation curve the shear rate, $S > 0.5$ and for a continually rising rotation curve the shear rate, $S < 0.5$. Following the method described by Seigar et al. (2006) we measure the shear at a 10 kpc radius. For M31, $1'$ is equivalent to 228 pc (Athanassoula & Beaton 2006; Holland 1998), and so 10 kpc is equivalent to $43.9'$. The shear is measured using the prescription described by Seigar (2005) and Seigar et al. (2004, 2005, 2006). In this method an average slope is fit to the outer part of the rotation curve (i.e., past the solid-body rotation regime), and the shear is then calculated at the given radius. For M31, at a radius of 10 kpc, the shear is $S = A/\omega = 0.54 \pm 0.02$.

There is little scatter in the correlation shear rate and pitch angle, and the line of best fit is given by

$$P = (64.24 \pm 2.87) - (73.24 \pm 5.53)S, \quad (6)$$

where P is the spiral arm pitch angle in degrees and

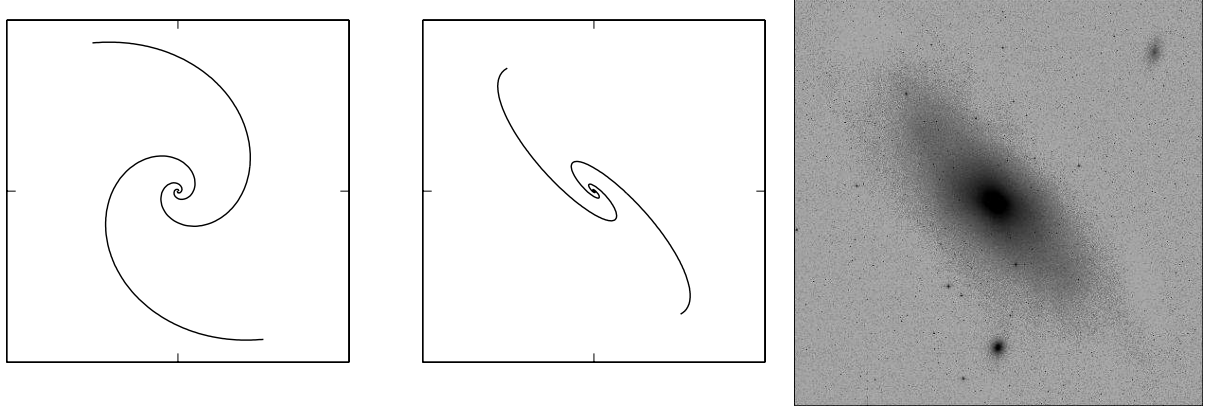


FIG. 6.— *Left:* A two-armed spiral viewed face-on with pitch angle, $P = 24.7^\circ$, as predicted for M31. *Center:* A spiral with pitch angle, $P = 24.7^\circ$, viewed with the inclination and position angle of M31. *Right:* 2MASS K_s -band image of M31.

S is the shear. From this the pitch angle for M31 is $P = 24.7 \pm 4.4^\circ$. (It should be noted that the shear at 10 kpc determined for the M1 B86 model in section 2.2 is $S = 0.52$ and for M1 G05 is $S = 0.56$. These estimates are consistent with the shear measured here. They results in pitch angles of $P = 26.2 \pm 2.2^\circ$ and $P = 23.2 \pm 2.0^\circ$ respectively, both of which are consistent with the pitch angle derived above).

Assuming a logarithmic spiral (see e.g., Seigar & James 1998b for the equations that define a logarithmic spiral), the spiral arm pattern of M31 is calculated. Figure 6 shows the predicted spiral arm pattern of M31 for a face-on view (*left*) and with an inclination angle, $i = 77.5^\circ$, and a position angle 45° (de Vaucouleurs et al. 1991) appropriate for M31 (*center*). This spiral arm pitch angle is larger than the H I spiral arm pitch angle of 16° calculated by Braun (1991), although it is possible that the spiral arm pattern in the neutral gas may be a few degrees tighter than that observed in the underlying stellar distribution. Furthermore, a pitch angle of 16° also lies just within the scatter of the spiral arm pitch angle versus rotation curve shear correlation when the shear, $S = 0.54$ (see Figure 3 of Seigar et al. 2006).

It is important to note that the spiral arm pattern shown in Figure 6 does not take into account the disk scale height and how broad the arms are. These plots are intended to illustrate how tightly wound the arm pattern would be if viewed from face-on. When viewed close to edge-on (as is the case for M31), the scale height of the disk and breadth of the spiral arms make it virtually impossible to determine the spiral arm pitch angle directly.

4. SUMMARY

In this paper we have derived a new mass model for M31, based on an updated baryonic contribution to the rotation curve. The baryonic contribution is derived using a K_s -band image and M/L ratios from Bell et al. (2003). Our mass model is in good agreement with the mass distribution derived from various observational methods. Our estimate of the halo virial mass, $M_{\text{vir}} = (8.7 \pm 0.7) \times 10^{11} M_\odot$ is in close agreement with the virial mass of $\sim 8 \times 10^{11} M_\odot$ found via kinematics of satellite galaxies (Côté et al. 2000) and the Andromeda

Stream (Geehan et al. 2006).

It is interesting to note that, while it has been shown that adiabatically contracted halo models do not generally fit the observed rotation curves of galaxies (e.g., Dutton et al. 2005, 2006; Kassin et al. 2006a, b; Pizagno et al. 2005), the observed rotation curve of a well-studied galaxy such as M31 is more consistent with a halo that has undergone adiabatic contraction than one that has not. Indeed, such a scenario is in agreement with the results of Klypin et al. (2002).

Much of the power in this analysis came from studying the normalization *and* outer slope of M31's rotation curve. This highlights the usefulness of extended rotation curve data in constraining general models of galaxy formation. Studies that test the applicability of adiabatic contraction often make use of large samples of galaxies that are dominated by late-type disk-dominated galaxies, with small bulges or no bulge at all. (e.g. Pizagno et al. 2005; Dutton et al. 2005, 2006; Gnedin et al. 2006; Kassin et al. 2006a, b). These bulgeless galaxies also tend to have very flat (or even rising) rotation curves, and it is therefore easy to explain these galaxy rotation curves without any need for adiabatic contraction. However, we suggest that early-type disk galaxies (e.g. Hubble types Sa–Sb), which have bulge-dominated centers, and rotation curves that fall-off due to the presence of a large bulge, may require adiabatic contraction. Although we have studied very few galaxies so far (M31 in this paper and two other galaxies in Seigar et al. 2006) our results indicate that in cases where rotation curves have a fall-off (two out of three cases), adiabatic contraction is needed. This may be true for all galaxies with large bulges. If so, it may favor a secular (rather than merger-driven) origin for these bulge-dominated systems, as the gradual accumulation of central mass increases the likelihood that AC will operate.

Support for this work was provided by NASA through grant number HST-AR-10685.01-A from the Space Telescope Science Institute, which is operated by the Association of Universities for Research in Astronomy, Inc., under NASA contract NAS5-26555. This publication makes use of data products from the Two Micron All

Sky Survey, which is a joint project of the University of Massachusetts and the Infrared Processing and Analysis Center/California Institute of Technology, funded by the National Aeronautics and Space Administration and the National Science Foundation. This research has made use of the NASA/IPAC Extragalactic Database (NED) which is operated by the Jet Propulsion Laboratory, California Institute of Technology, under contract with the National Aeronautics and Space Administration. The authors wish to thank the anonymous referee whose comments and suggestions were extremely useful in the preparation of this paper. The authors also wish to thank Tom Jarrett and Luis Ho for their discussions.

REFERENCES

- Alam, S. M. K., Bullock, J. S., & Weinberg, D. H. 2002, *ApJ*, 572, 34
- Andredakis, Y. C., Peletier, R. F., & Balcells, M. 1995, *MNRAS*, 275, 874
- Athanassoula, E., & Beaton, R. L. 2006, *MNRAS*, 370, 1499
- Barnes, J. E. 1987, in *Nearly Normal Galaxies: From the Planck Time to the Present*, ed. S. M. Faber et al. (New York: Springer Verlag), 154
- Beaton, R. L., et al. 2006, *ApJ*, submitted (astro-ph/0605239)
- Bell, E. F., & de Jong, R. S. 2001, *ApJ*, 550, 212
- Bell, E. F., McIntosh, D. H., Katz, N., & Weinberg, M. D. 2003, *ApJ*, 585, 117
- Bender, R., et al. 2005, *ApJ*, 631, 280
- Benson, A. J., Bower, R. G., Frenk, C. S., Lacey, C. G., Baugh, C. M., & Cole, S. 2003, *ApJ*, 599, 38
- Bertin, E., & Arnouts, S. 1996, *A&AS*, 117, 393
- Blais-Ouellette, S., Amram, P., & Carignan, C. 2001, *AJ*, 121, 1952
- Blumenthal, G. R., Faber, S. M., Flores, R., & Primack, J. R. 1986, *ApJ*, 301, 27
- Bullock, J. S., Dekel, A., Kolatt, T. S., Kravtsov, A. V., Klypin, A. A., Porciani, C., & Primack, J. R. 2001a, *ApJ*, 555, 240
- Bullock, J. S., Kolatt, T. S., Sigad, Y., Somerville, R. S., Kravtsov, A. V., Klypin, A. A., Primack, J. R., & Dekel, A. 2001b, *MNRAS*, 321, 559
- Braun, R. 1991, *ApJ*, 372, 54
- Brinks, E., & Burton, W. B. 1984, *A&A*, 141, 195
- Caon, N., Capaccioli, M., & D'Onofrio, M. 1993, *MNRAS*, 265, 1013
- Capaccioli, M. 1989, in *The World of Galaxies*, ed. H. G. Corwin, & L. Bottinelli (Berlin: Springer-Verlag), 208
- Carignan, C., Chemin, L., Huchtmeier, W. K., & Lockman, F. J. 2006, *ApJ*, 641, L109
- Cembranos, J. A., Feng, J. L., Rajaraman, A., & Takayama, F. 2005, *Phys. Rev. Lett.*, 95, 181301
- Chapman, S. C., Ibata, R., Lewis, G. F., Ferguson, A. M. N., Irwin, M., McConnachie, A., & Tanvir, N. 2006, *ApJ*, in press (astro-ph/0602604)
- Ciotti, L. 1991, *A&A*, 249, 99
- Cole, S., Lacey, C. G., Baugh, C. M., & Frenk, C. S. 2000, *MNRAS*, 319, 168
- Choi, J.-H., Lu, Y., Mo, H. J., & Weinberg, M. D. 2006, *MNRAS*, in press (astro-ph/0604587)
- Côté, P., Mateo, M., Sargent, W. L. W., & Olszewski, E. W. 2000, *ApJ*, 537, L91
- de Jong, R. S., 1996, *A&AS*, 118, 557
- de Vaucouleurs, G. 1948, *Ann. Astrophys.*, 11, 247
- de Vaucouleurs, G. 1959, *Handbuch der Physik*, 53, 275 & 311
- de Vaucouleurs, G., de Vaucouleurs, A., Corwin, H. G., Buta, R. J., Paturel, G., & Fouqué, P. 1991, *The Third Reference Catalog of Bright Galaxies*, (New York: Springer) (RC3)
- D'Onofrio, M. 2001, *MNRAS*, 326, 1517
- Dehnen, W., McLaughlin, D. E., Sachania, J. 2006, *MNRAS*, 369, 1688
- Dutton, A. A., Courteau, S., de Jong, R., & Carignan, C. 2005, *ApJ*, 619, 218
- Dutton, A. A., van den Bosch, F. C., Dekel, A., & Courteau, S. 2006, *ApJ*, submitted (astro-ph/0604553)
- Einasto, J. 1972, in *IAU Symp. 144, External Galaxies and Quasi-Stellar Objects*, ed. D. E. Evans (Dordrecht: Reidel), 37
- Evans, N. W., & Wilkinson, M. I. 2000, *MNRAS*, 316, 929
- Fardal, M. A., Babul, A., Geehan, J. J., & Gahathakurta, P. 2006, *MNRAS*, 366, 1012
- Flores, R. A., & Primack, J. R. 1994, *ApJ*, 427, L1
- Flores, R., Primack, J. R., Blumenthal, G. R., & Faber, S. M. 1993, *ApJ*, 412, 443
- Geehan, J. J., Fardal, M. A., Babul, A., & Gahathakurta, P. 2006, *MNRAS*, 366, 996
- Gnedin, O. Y., Kravtsov, A. V., Klypin, A. A., & Nagai, D. 2004, *ApJ*, 616, 16
- Gnedin, O. Y., Weinberg, D. H., Pizagno, J., Prada, F., & Rix, H.-W. 2006, *ApJ*, submitted (astro-ph/0607394)
- Gonzalez, A. H., Williams, K. A., Bullock, J. S., Kolatt, T. S., & Primack, J. R. 2000, *ApJ*, 528, 145
- Graham, A. W. 2001, *AJ*, 121, 820
- Graham, A. W., & Driver, S. 2005, *PASA*, 22, 118
- Holland, S. 1998, *AJ*, 115, 1916
- Humphrey, P. J., Buote, D. A., Gastaldello, F., Zappacosta, L., Bullock, J. S., Brightenti, F., & Mathews, W. G. 2006, *ApJ*, 646, 899
- Jarrett, T. H., Chester, T., Cutri, R., Schneider, S. E., & Huchra, J. P. 2003, *AJ*, 125, 525
- Jedrzejewski, R. I. 1987, *MNRAS*, 226, 747
- Jesseit, R., Naab, T., & Burkert, A. 2002, *ApJ*, 571, L89
- Kaplinghat, M., Knox, L., & Turner, M. S. 2000, *Phys. Rev. Lett.*, 85, 3335
- Kaplinghat, M. 2005, *Phys. Rev. D*, 72, 063510
- Kassin, S. A., de Jong, R. S., & Pogge, R. W. 2006a, *ApJS*, 162, 80
- Kassin, S. A., de Jong, R. S., & Weiner, R. J. 2006b, *ApJ*, 643, 804
- Kent, S. M. 1989, *AJ*, 97, 1614
- Kent, S. M., Huchra, J. P., & Stauffer, J. 1989, *AJ*, 98, 2080
- Khosroshahi, H. G., Wadadekar, Y., & Kembhavi, A. 2000, *ApJ*, 533, 162
- Klypin, A., Zhao, H., & Somerville, R. S. 2002, *ApJ*, 573, 597
- Kuzio de Naray, R., McGaugh, S. S., de Blok, W. J. G., & Bosma, A. 2006, *ApJS*, 165, 461
- Light, E. S., Danielson, R. E., & Schwarschild, M. 1974, *ApJ*, 194, 257
- Loinard, L., Allen, R. J., & Lequeux, J. 1995, *A&A*, 301, 68
- Macciò, A. V., Moore, B., Stadel, J., & Diemand, J. 2006, *MNRAS*, 366, 1529
- Möllenhoff, C., & Heidt, J. 2001, *A&A*, 368, 16
- Moore, B. 1994, *Nature*, 370, 629
- Moore, B., Quinn, T., Governato, F., Stadel, J., & Lake, G. 1999, *MNRAS*, 310, 1147
- Navarro, J. F., Frenk, C. S., & White, S. D. M. 1997, *ApJ*, 462, 563 (NFW)
- Pizagno, J., et al. 2005, *ApJ*, 633, 844
- Prugniel, P., & Simien, F. 1997, *A&A*, 321, 111
- Rubin, V. C., & Ford, W. K. 1970, *ApJ*, 159, 379
- Ryden, B. S., & Gunn, J. E. 1987, *ApJ*, 318, 15
- Seigar, M. S., & James, P. A. 1998a, *MNRAS*, 299, 672
- Seigar, M. S., & James, P. A. 1998b, *MNRAS*, 299, 685
- Seigar, M. S., Block, D. L., & Puerari, I. 2004, in *Penetrating Bars Through Masks of Cosmic Dust*, ed. D. L. Block et al. (Dordrecht: Springer), 155
- Seigar, M. S. 2005, *MNRAS*, 361, L20
- Seigar, M. S., Block, D. L., Puerari, I., Chorney, N. E., & James, P. A. 2005, *MNRAS*, 359, 1065
- Seigar, M. S., Bullock, J. S., Barth, A. J., & Ho, L. C. 2006, *ApJ*, 645, 1012
- Sellwood, J. A., & McGaugh, S. S. 2005, *ApJ*, 634, 70
- Sérsic, J.-L. 1963, *Boletin de la Asociacion Argentina de Astronomia*, 6, 41
- Sérsic, J.-L. 1968, *Atlas de Galaxias Australes (Cordoba: Observatorio Astronomico)*

- Simon, J. D., Bolatto, A. D., Leroy, A., Blitz, L., & Gates, E. L. 2005, *ApJ*, 621, 757
- Sofue, Y., & Kato, T. 1981, *PASJ*, 33, 449
- Somerville, R. S., & Primack, J. R. 1999, *MNRAS*, 310, 1087
- Strigari, L. E., Kaplinghat, M., & Bullock, J. S. 2006, *Phys. Rev. Lett.*, submitted (astro-ph/0606281)
- Swaters, R. A., Madore, B. F., van den Bosch, F. C., & Balcells, M. 2003, *ApJ*, 583, 732
- Tully, R. B., & Fisher, J. R. 1977, *A&A*, 54, 661
- van den Bosch, F. C., & Swaters, R. A. 2001, *MNRAS*, 325, 1017
- Walterbos, R. A. M., & Kennicutt, R. C. 1987, *A&AS*, 69, 311
- Weinberg, D. H., Colombi, S., Davé, R., & Katz, N. 2006, *ApJ*, submitted (astro-ph/0604393)
- Yang, X., Mo, H. J., & van den Bosch, F. C. 2003, *MNRAS*, 339, 1057
- Zappacosta, L., Buote, D. A., Gastaldello, F., Humphrey, P. J., Bullock, J., Brighenti, F., & Mathews, W. 2006, *ApJ*, in press (astro-ph/0602613)
- Zentner, A. R., & Bullock, J. S. 2002, *Phys. Rev. D*, 66, 043003